

## Appraising the Risk Assessment of Non-Structural Components via Simplified and Machine-Learning-Based Approaches

Davit Shahnazaryan & Gerard J. O'Reilly

**To cite this article:** Davit Shahnazaryan & Gerard J. O'Reilly (12 Feb 2024): Appraising the Risk Assessment of Non-Structural Components via Simplified and Machine-Learning-Based Approaches, *Journal of Earthquake Engineering*, DOI: [10.1080/13632469.2024.2314169](https://doi.org/10.1080/13632469.2024.2314169)

**To link to this article:** <https://doi.org/10.1080/13632469.2024.2314169>



Published online: 12 Feb 2024.



Submit your article to this journal



View related articles



View Crossmark data



# Appraising the Risk Assessment of Non-Structural Components via Simplified and Machine-Learning-Based Approaches

Davit Shahnazaryan  and Gerard J. O'Reilly 

Centre for Training and Research on Reduction of Seismic Risk (ROSE Centre), Scuola Universitaria Superiore IUSS Pavia, Pavia, Italy

## ABSTRACT

Uncertainties in building element modelling and ground motions are indispensable for rigorous seismic risk quantification. demand–intensity models simply relate building performance to intensity and subsequently risk. This article describes developments toward non-structural element (NSEs) risk quantification. The demand–intensity models are applied to infilled reinforced concrete (RC) case-study buildings. Implicit and explicit NSE numerical modelling is used to validate the models versus the direct integration of risk exceedance. For faster estimation techniques, machine learning models are trained to estimate the demand–intensity model fitting parameters on a modest dataset of RC infilled buildings. Among these, the extreme gradient boosting (XGBoost) demonstrated superior performance, indicating further possible directions for improvement where larger datasets are available. These models facilitate the simple retrieving of demand–intensity models without extensive structural analysis and can be utilized for both structural and non-structural elements when assessing risk in single or multiple buildings as part of portfolio analysis.

## ARTICLE HISTORY

Received 23 November 2022  
Accepted 30 January 2024

## KEYWORDS

Seismic risk; non-structural elements; demand-intensity; RC buildings; machine learning

## 1. Introduction

Proper quantification of collapse risk, as well as incurred losses of buildings following ground motion shaking, is of high importance within the earthquake engineering community. While ensuring collapse safety and avoiding loss of life is at the forefront of seismic engineering objectives, significant advances are still needed toward reducing the losses incurred by damaged non-structural elements (NSEs). Multiple studies have shown that a substantial portion of economic losses are associated with NSE damage following numerous earthquakes (Filiatrault et al. 2001; O'Reilly et al. 2018; Perrone et al. 2019; Ricci, de Luca, and Verderame 2011), which is not surprising given that the most significant portion of monetary investments in typical buildings is associated with NSEs (Taghavi and Miranda 2004). Most cases are tied to buildings designed following outdated design codes where seismic design may or may not have been provisioned. Likewise, new designs tend to show a lack of adequate consideration of NSE performance, resulting in downtime due to failed mechanical or electrical components, notwithstanding the satisfactory performance of structural elements, inhibiting continuous use and immediate occupancy following earthquake shaking (Filiatrault and Sullivan 2014). Traditionally, seismic design codes have two main objectives: (1) life safety through prevention of structural collapse; and (2) some checks at frequent levels of ground shaking to mitigate excessive storey drifts and floor accelerations, implicitly avoiding extensive NSE damage, taken as a proxy for economic losses. Due to the NSEs having lower inherent strength and ductility compared to structural elements, they tend to be damaged during more frequent ground shaking resulting in direct losses.

Direct methods whereby non-structural elements are explicitly modelled along with the structure were investigated by Wanitkorkul and Filiatral (2008). In addition, an alternative approach considering the interaction of elements in an un-coupled (implicit) manner was employed elsewhere (Merino Vela, Brunesi, and Nascimbene 2019). With the increased popularity of risk-targeted design methods in ensuring uniform structural behaviour in terms of collapse safety (Aschheim and Black 2000; Cornell 1996; O'Reilly and Calvi 2019; Žižmond and Dolšek 2019), as well as design methods ensuring uniform economic loss (Krawinkler et al. 2006; Shahnazaryan, O'Reilly, and Monteiro 2022) following simplified methodologies, similar methods are explicitly needed for NSEs. For example, for characterising seismic risk in Italy in a simple and communicable manner, the *Sismabonus* guidelines (Cosenza et al. 2018) were introduced in 2017, where the seismic risk of buildings is classified into various ratings using the more critical of collapse safety index and expected annual loss ratio. Pertaining to NSEs specifically, O'Reilly and Calvi (2021) outlined a seismic classification scheme similar to *Sismabonus*, where demand-intensity models were employed to characterise the seismic performance of both drift- and acceleration-sensitive NSEs.

This article explores the use of demand-intensity models to quantify NSE behaviour in terms of engineering demand parameters (EDPs) of maximum peak storey drift (MPSD) and maximum peak floor acceleration (MPFA), which are then used to calculate the mean annual frequency of exceedance (MAFE), or risk of a given limit or damage state being violated in the NSEs. demand-intensity models are functions representing a relationship between structural demand and seismic intensity and have shown good conformance when compared to non-linear time history analysis (NLTHA) results (O'Reilly and Calvi 2021; O'Reilly and Monteiro 2019). Generalising demand-intensity models could be a cumbersome task necessitating big datasets based on NLTHA results. Additionally, such models will ideally be generated for a portfolio of buildings sharing similar characteristics; however, to further underline the applicability of the demand-intensity models, machine learning (ML) models were trained on a dataset comprising NLTHA results of many buildings. The relevance of ML approaches in view of growing datasets has been explored in past studies for seismic analysis and structural response prediction (Conte, Durrani, and Shelton 1994; Ferrario et al. 2017; Huang and Burton 2019; R. Zhang et al. 2019), risk assessment (Gentile and Galasso 2022) as well as structural safety (Y. Zhang et al. 2018) with varying success in predicting underlying relationships between input and response variables. These studies generally looked at predicting a single variable through either regression or classification or a combination of the two. In contrast, the methods employed here aim to predict multiple dependent variables through regression instead of one variable characterising the structural behaviour associated with varying intensity levels. In other words, the ML approaches were employed to establish demand-intensity models of buildings based on results attained via NLTHA with a view to expediting this process whilst still leaving the actual risk quantification customisable and flexible depending on the risk analyst's needs.

With these objectives in mind, a case study reinforced concrete (RC) infilled building configuration was designed (Nafeh and O'Reilly 2022) and non-linear models were generated to apply multiple stripe analysis (MSA) (Jalayer 2003). Models were created with (explicit) and without (implicit) inclusion of NSE. Two types of NSE were utilized: acceleration- and drift-sensitive. Finally, buildings were assumed to be located in one of two site locations in Italy with varying seismicity. Similarly, a dataset containing multiple site locations, code level, and configurations of RC buildings with masonry infills were used to train ML models outlined.

The following methods have been employed within this study: parametric approaches such as multiple multivariate ridge and lasso regression, non-parametric approaches such as decision tree (DT), K-nearest neighbor regression (KNN), support vector regression (SVR) and extreme gradient boosting (XGBoost) (Chen and Guestrin 2016). Additionally, a stacked generalization model (Wolpert 1992) combined the predictions from multiple ML models on the dataset. To avoid assigning the same importance to all independent variables in the prediction model akin to logic tree weight, resulting in low bias and high variance, ridge or lasso regression were used, where the regression coefficients are shrunk via a penalty on their size. The penalties aid in removing the variables with less influence on the



prediction model. Parametric approaches assume normality of distribution of independent variables and linear relationship between the independent and dependent variables. However, this might not be the case; therefore, non-parametric approaches are also used. DT uses a tree-like model of decisions, where each decision depends on one or more independent variables. The tree's base is the root node, from where the tree is split into decision nodes flowing into leaf nodes representing the consequences of the decisions. Each decision is a split point, and the leaf nodes are proxies for predictions. This method is based on bootstrap aggregation or bagging that uses sub-samples to construct the decision trees and make the final prediction as the average of predictions of all trees. KNN regression uses the variable similarity technique to make predictions. The data points are assigned values based on how closely they resemble the points in the training set. In contrast to other regression models, SVR tries to fit the best line within a threshold value, which is the distance between the hyperplane and boundary line. The objective of the SVR is to minimise the l2-norm of the coefficient vector. The absolute error is set to be less or equal to a specified threshold value, which is tuned for the desired accuracy of the model. XGBoost is an advancement of gradient boosted decision tree algorithms for faster speed and better performance. It uses parallel trees as opposed to traditional gradient boosting. Boosting is an ensemble technique of adding new models to correct the residuals made by past models. Those models were added sequentially until no further improvements were made. Essentially, the residuals of previous models were computed and combined for a final improved prediction. It uses a gradient descent algorithm to minimise the loss when adding new models.

Additionally, a stacked generalization model (Wolpert 1992) is used, which involves combining the predictions from multiple ML models on the dataset. XGBoost and stacked generalisation are ensemble methods where new models learn how to best combine predictions from numerous previous models. Additionally, to understand the relationships between variables, the SHapley Additive exPlanations approach (SHAP) (Lundberg and Lee 2017) was used to rank the input variables and understand the effects of different variables on the fitting parameters. To this end, the demand-intensity and ML models foresee higher accuracies and ease of generalization of demand-intensity models for portfolio of buildings trained on datasets containing pre-design and/or minimal design characteristics of buildings, all of which contribute towards a more simplified and expedite quantification of seismic risk in buildings.

## 2. Simplified Risk Calculation

### 2.1. Linear Demand–Intensity Model

By extending simplified methods of analysis for RC buildings, O'Reilly and Calvi (Jalayer 2003; O'Reilly and Calvi 2020), among others, used demand–intensity models (Fig. 1) characterized via closed-form solutions to assess and verify structures for storey drift and floor acceleration demands in a risk-oriented manner. For a given MPSD,  $\theta_{\max}$ , where the mechanism for a ductile structure is expected to be a first mode-based beam-sway mechanism, and in some cases for a given MPFA,  $a_{\max}$ , the median demand–intensity relationship can be represented as linear in the logspace following Eq. (1) (Cornell et al. 2002).

$$D_{\max} \approx ms^b \quad (1)$$

where  $D_{\max}$  is either  $\theta_{\max}$  or  $a_{\max}$ ,  $s$  is the intensity measure (IM) level,  $m$  and  $b$  are fitting coefficients of structural analysis results which, in essence, define the model. When  $b$  is equal 1 consistent with equal displacement rule is achieved (Veletsos and Newmark 1960).

### 2.2. Bilinear Demand–Intensity Models

With regard to buildings exhibiting two distinct phases of response, O'Reilly and Monteiro (O'Reilly et al. 2018) described the bilinear demand–intensity relationship given in Eq. (2) (Fig. 1). A bilinear

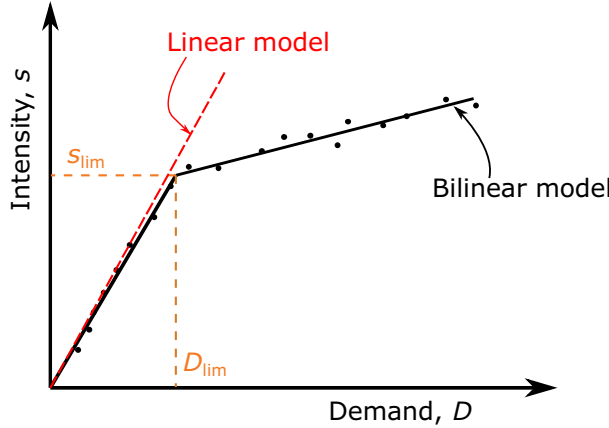


**Figure 1.** Illustrations of the demand–intensity models.

relationship was proposed due to the MPFA saturating with increasing intensity as a result of structural yielding, or when MPSD quickly accumulates following masonry infill collapse and subsequent change in the response mechanism, where a linear relationship is no longer sufficient. Additionally, the division of two zones of response may be considered more suitable for the mechanical behaviour of structures. It can be applicable for cases where the demand is saturated beyond a specific threshold as outlined above for the case of force-based demands like base shear or floor accelerations (O'Reilly et al. 2018).

$$D_{\max} \approx \begin{cases} m_{lower} s^{b_{lower}}, & s < s_{Limit} \\ m_{upper} s^{b_{upper}}, & s \geq s_{Limit} \end{cases} \quad (2)$$

where  $s_{limit}$  is the intensity limit when, for example, the masonry infills are expected to collapse, or in the case of MPFA, when structural yielding occurs, and likewise with the linear model  $m_{lower}$ ,  $m_{upper}$ ,  $b_{lower}$  and  $b_{upper}$  are fitting coefficients that define the model.

### 2.3. Risk Computation

To compute MAFE,  $\lambda$ , or risk, at a given limit state, Vamvatsikos (2013) expanded upon the work by Cornell et al. (2002) with the development of a closed-form expression for linear demand–intensity models given in Eq. (3) considering a refined site hazard curve defined via second-order fitting parameters  $k_0$ ,  $k_1$ , and  $k_2$ .

$$\lambda = \sqrt{\phi' k_0^{1-\phi'}} H \left( \left( \frac{D_{\max}}{m} \right)^{\frac{1}{b}} \right)^{\phi'} \exp \left( \frac{k_1^2 \phi'}{2b^2} \beta_{Tot}^2 \right) \quad (3)$$

where  $\phi'$  is given by Eq. (4):

$$\phi' = \frac{1}{1 + 2k_2 \beta_{Tot}^2 / b^2} \quad (4)$$

For the bilinear model described in Eq. (2) on the other hand, the MAFE is given by Eq. (5).

$$\lambda = F_{lower}(s_{limit}) \lambda_{lower} + [1 - F_{upper}(s_{limit})] \lambda_{upper} \quad (5)$$

where  $F_{lower}(s_{limit})$  and  $F_{upper}(s_{limit})$  are the lognormal cumulative density functions with corresponding mean values of  $\mu_{lower}$  and  $\mu_{upper}$  and standard deviations of  $\sigma_{lower}$  and  $\sigma_{upper}$ , respectively, which are

described in Eqs. (6) and (7), and  $\lambda_{\text{lower}}$  and  $\lambda_{\text{upper}}$  correspond to the estimates one obtains from Eq. (3) when using the corresponding fitting coefficients  $m$  and  $b$ .

$$\mu = \phi' \left( \frac{(\ln D_{\max} \ln m)}{b} - \frac{k_1 \beta_{\text{Tot}}^2}{b^2} \right) \quad (6)$$

$$\sigma = \frac{\beta_{\text{Tot}}^2 \sqrt{\phi'}}{b} \quad (7)$$

In both estimates of MAPE above, the term  $\beta_{\text{Tot}}$  represents the total expected uncertainty, or dispersion, in the EDP. This can arise from several sources and four general terms might be utilized, as given via the combination in Eq. (8). The  $\beta_{\text{DR}}$  and  $\beta_{\text{DU}}$  terms are associated with the natural randomness (i.e. aleatory uncertainty related to record-to-record variability) and inherent uncertainty (i.e. epistemic uncertainty typically associated with the modelling uncertainty) of the demand, respectively. Similarly, the  $\beta_{\text{CR}}$  and  $\beta_{\text{CU}}$  terms are associated with aleatory and epistemic uncertainties of the capacity. The total uncertainty, as a result, may be computed using Eq. (8) assuming a square root sum of square combination and taking each source as independent of one another.

$$\beta_{\text{Tot}} = (\beta_{\text{DR}}^2 + \beta_{\text{DU}}^2 + \beta_{\text{CR}}^2 + \beta_{\text{CU}}^2)^{0.5} \quad (8)$$

### 3. Demand–Intensity Model Fitting

#### 3.1. Design of Case-Study Buildings

For the application of demand–intensity models and validation through extensive non-linear dynamic analyses, a single non-ductile RC frame structure with masonry infills was adapted from the building database developed by Nafeh and O'Reilly (2022). The building is a four-storey structure, corresponding to index 4-D-SSD, and was designed to conform to the design code provisions of the mid-1970s and 1980s in Italy. Two building sites in Italy were selected: Milano, representing low seismicity, and L'Aquila for high seismicity to assess the results for different hazard levels. The considered building plan layout is given in Fig. 2 and consists of four identical storeys in terms of plan layout, each of 3.0 m in height. Infills were categorised as strong and medium depending on their strength and thickness, as per Hak et al. (2012). Out-of-plane failure mechanisms of the infills were not considered in the analysis. Additionally, Fig. 2 displays the distribution of gypsum partitions within the individual apartments of the building. Further details on the structural layout and its design can be found in Nafeh and O'Reilly (2022).

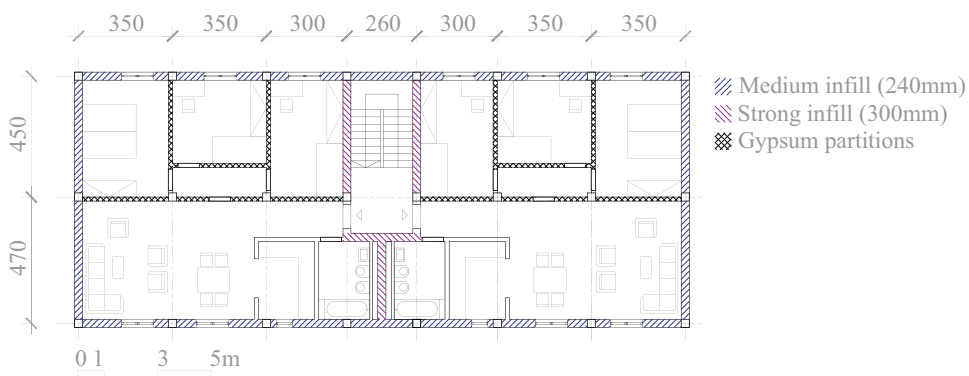


**Figure 2.** Building plan layout.

Structural models were created without NSE modelling (implicit) and with the explicit modelling of NSE. The buildings were analysed via MSA, and the median MPSD and MPFA were used to fit the demand-intensity models described in Sections 2.1 and 2.2. NSE risk computation was carried out using the procedures outlined in Section 2.3, and the final results will be compared in Section 4 between the implicit and explicit modelling approaches to examine any potential impact of this choice on risk estimates.

### 3.2. Numerical Modelling Approach

OpenSees (McKenna, Scott, and Fenves 2010) was used to create the numerical models of the case study building. In the case of the implicit approach, the performance of NSE was assessed based on the structure's response at a specific storey level. This means that NSEs were not directly incorporated into the non-linear structural model in OpenSees, and the demands on the NSEs were simply inferred from the structural response, assuming that the NSEs would have no impact on the overall behaviour. In contrast for the explicit modelling, the NSEs were directly modeled, and the coupled response of the NSE and the structure was assessed.

Two types of NSE were considered within the building. The first was cold-formed steel framed gypsum partition walls with full connections as they are susceptible to damage due to drift. The second was a vibration isolated chiller sensitive to damage due to floor acceleration. For the gypsum partitions, these were considered along both directions of the building and at all storeys. The relative distribution of the NSEs within the building with corresponding references for fragility functions are given in Fig. 2 and Table 1. At the same time, a single unit of chiller is assumed to be placed on the roof of the building. The chiller corresponds to the identification of D3031.012b present in FEMA P58-3 (FEMA 2012). The gypsum partitions are counted using meters (per m) as the unit of measure. It is assumed that there are 23.55 m gypsum partitions in longitudinal direction and 12.6 m in the transverse direction.

Institutional cold-formed steel framed gypsum partition walls with full connections adopted from Retamales et al. (2011) were considered within the case study building. The gypsum partitions were distributed along both directions of the case study building and at all storeys, as given in Table 1 and Fig. 2. The non-linear models were created through Pinching4 material models in OpenSees (McKenna, Scott, and Fenves 2010) to characterise the Wayne Stewart degrading stiffness hysteresis model (Stewart 1987). Partition walls are characterised as a simple spring in the longitudinal direction, while the out-of-plane behaviour of partition walls was not considered. As noted in Retamales et al. (Retamales et al. 2011) the out-of-plane stiffness is around 10% of the in-plane partition wall stiffness, which is negligibly low for the behaviour of a building-partition wall system.

Similar to drift-sensitive elements of gypsum partition walls, an acceleration-sensitive element of a chiller of less than 100-ton capacity was adopted from FEMA P58-3 (FEMA 2012) and placed on the roof of the case study building. Based on its capacity, it was inferred from available data and modelled as a 7-ton mass (amounting to 0.9% of the mass of the building) on springs characterised via  $4 \times 0.5\text{kN/mm}$  horizontal stiffness using OpenSees (Mazzoni et al. 2006). Given the small NSE to building mass ratio, the dynamic response of the explicit model is expected to not vary significantly from the implicit model. Based on a sensitivity study, whereby the mass of the chiller was continuously

**Table 1.** Mean quantities and fragility functions of the damageable NSEs of the case study building in the longitudinal direction (quantities for transverse direction listed in parenthesis).

| Element              | Reference for fragility function | Median, $\eta_c$ | Dispersion, $\beta_{CR}$ | Demand parameter | Unit     | Location and Quantity    |
|----------------------|----------------------------------|------------------|--------------------------|------------------|----------|--------------------------|
| Gypsum partition     | Retamales et al. (2013).         | 0.88%            | 0.33                     | MPSD [%]         | per m    | All storeys, 23.55(12.6) |
| Chiller (D3031.012b) | FEMA P58-3 (2012)                | 0.43g            | 0.60                     | MPFA [g]         | per unit | Roof, 1                  |

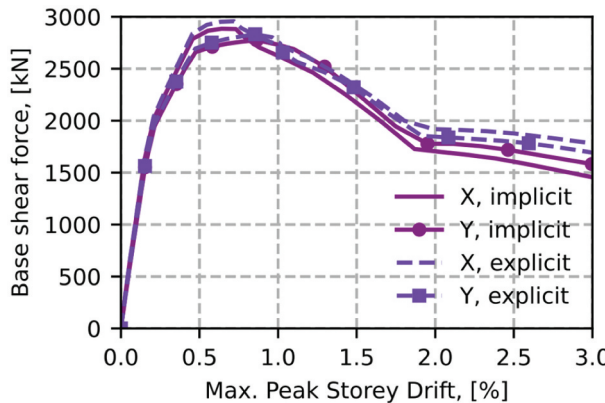


**Figure 3.** Pushover curves in both directions of the building with and without explicit consideration of NSE during modelling.

increased, and the elastic vibration periods and mode shapes were monitored, it begins to have a notable impact when this mass ratio increases to around 2.0% of the building mass. Its effects on risk outputs will be examined in the next section.

Pushover analyses were then conducted for both implicit and explicit modelling approaches and the results are shown in Fig. 3. There is a slight variation between the implicit models and the models with partition walls explicitly modeled underlining a slight increase in strength and stiffness. The focus of the next section will be whether such differences in modelling consideration will have any notable impact on the risk estimates obtained and how any discrepancies compare to the simplified procedures.

### 3.3. Record Selection

For what concerns the IM to adopt as part of MSA, recent research (Baker 2011; Eads, Miranda, and Lignos 2015; O'Reilly 2021) has shown that using  $Sa(T_1)$  may not be the most robust approach for the building typology studied here. The spectral acceleration at some multiple of the fundamental period,  $T_1$ , or averaged range around it may be used (Baker 2011). Eads, Miranda, and Lignos (2015) have shown that the spectral acceleration averaged over a period range around  $T_1$ ,  $Sa_{avg}$ , is an efficient IM in collapse risk estimation. Therefore, for assessment purposes, probabilistic seismic hazard assessment (PSHA) was performed using OpenQuake (Pagani et al. 2014) with the SHARE hazard model (Woessner and Wiemer 2005) for the selected sites of Milano (low) and L'Aquila (high) with site characteristics presented in Mori et al. (2020) and using  $Sa_{avg}$  as an IM (Fig. 4). A set of 40 ground motion record pairs were selected from the NGA West-2 database (Ancheta et al. 2014) using the conditional spectrum approach (Kohrangi et al. 2017) with each record's soil type being consistent with the site. The geometric mean of the ground motion's pair was considered for the selection, where the scale factors of the records were limited to 3.5 to mitigate possible issues of bias (Dávalos and Miranda 2019). Eleven return periods were used to conduct MSA and characterise the structural response of the case study buildings from initial damage of masonry infills to global structural collapse. The response of the principal direction exhibiting the lowest ductility was used as the primary indicator of structural behaviour.

## 4. NSE Performance Assessment

### 4.1. Implicit NSE Performance Assessment

To validate the performance of NSEs under seismic excitation, the case study RC infilled building was analysed via MSA following the record selection procedure outlined in Section 3.3.  $Sa_{avg}$  was used to

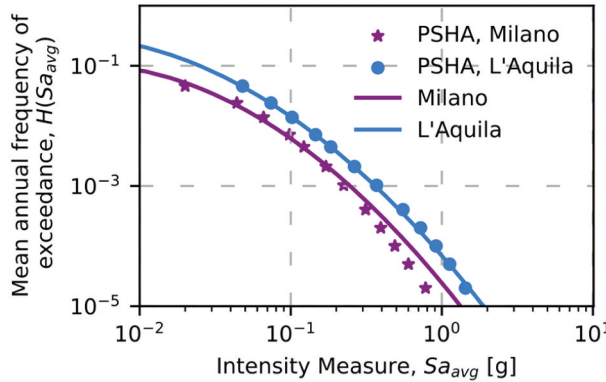


**Figure 4.** Seismic hazard corresponding to  $Sa_{avg}$  for both sites.

represent the seismic intensity with 5% damping in both principal directions of the building. The median response was computed using the MSA results, and the results are provided in Fig. 5. In the case of MPSD response and as a result of a non-ductile mechanism,  $\theta_{lim}$  was identified, corresponding to the point of interaction of two distinct zones of response to characterise the bilinear demand–intensity model, as outlined in Section 2.2. Here,  $\theta_{lim}$  corresponds to the nominal collapse point of masonry infills. This point is not fixed but is instead optimised to achieve better fits for both distinct branches of a bilinear function.

The sample computations of MAFE and the return period of loss of functionality of those elements at the “collapsing, requiring total replacement” and “inoperable” damage states for the gypsum partitions and a chiller, respectively, are given in Table 2. Following the expressions outlined in Section 2, representing the demand–intensity models and risk calculations, it is relatively simple to perform computations of MAFE associated with a particular NSE damage state. Uncertainties in the characterisation of NSE capacity and structural seismic behaviour were propagated and accounted for in the computations. The dispersion in demand was denoted as  $\beta_{DR} \approx \beta_{IM,R} \times b$ , where  $\beta_{IM,R}$  is the dispersion in intensity required to exceed a given demand threshold, which is inferred from the MSA results in Fig. 5. Additionally, the risk estimate was appraised through direct integration of MSA results with the seismic hazard illustrated in Fig. 4. Relatively good matching was achieved in terms of risk between both direct integration of MSA results and the simpler demand–intensity model-based method. The main difference in MAFE stems from the variation of IM and  $\beta$  values used following the simplified demand–intensity

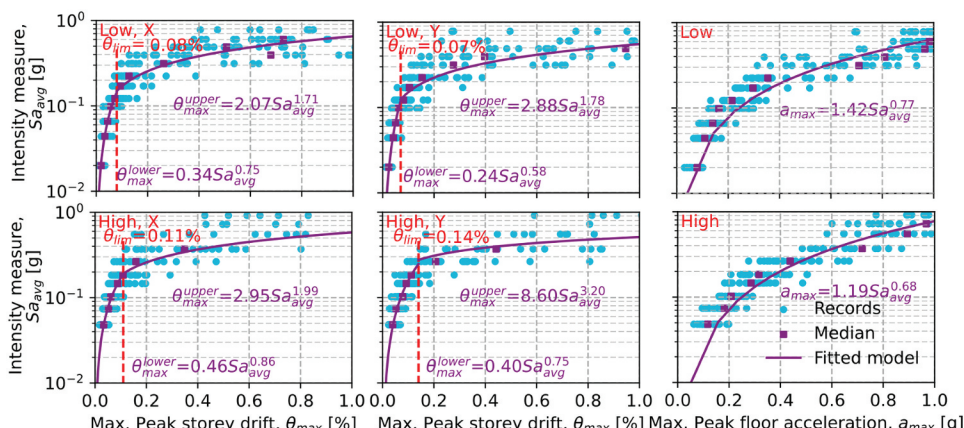


**Figure 5.** Results of MSA and demand–intensity models of MPSD and MPFA for low and high seismicity sites fitted for values of  $Sa_{avg}$ .

**Table 2.** Sample computation of MAFE and return period of loss of functionality following the simplified approach for the high seismicity site.

| MPSD-sensitive   | MPFA-sensitive   |
|--|--|
| Along X direction  | Non-directional factor=1.0                                     |
| $\eta_c = 0.88\%$ , $\beta_{CR,\theta} = 0.33$ , $\beta_{CU,\theta} = 0.0$ | $\eta_c = 0.43g$ , $\beta_{CR,a} = 0.6$ , $\beta_{CU,a} = 0.0$ |
| $m_{\theta,lower} = 0.46$ , $b_{\theta,lower} = 0.86$ ,                    | $m_a = 1.19$ , $b_a = 0.68$ ,                                  |
| $m_{\theta,upper} = 2.95$ , $b_{\theta,upper} = 1.99$ ,                    | $\beta_{DR,IM} = 0.25$ , $\beta_{DU,IM} = 0.3$                 |
| $\beta_{DR,IM} = 0.54$ , $\beta_{DU,IM} = 0.3$                             |  |
| $\beta_{TOT,\theta,lower} = 0.42$ , $\beta_{TOT,\theta,upper} = 1.36$      | $\beta_{TOT,a} = 0.70$   |
| $k_0 = 68.9 \times 10^{-6}$ , $k_1 = 2.88$ , $k_2 = 0.25$                  |  |
| $\varphi'_{a,lower} = 0.783$ , $\varphi'_{a,upper} = 0.855$ ,              | $\varphi'_a = 0.661$   |
| $\mu_{lower} = -0.677$ , $\mu_{upper} = -1.365$ ,                          |  |
| $\sigma_{lower} = 0.427$ , $\sigma_{upper} = 0.631$                        |  |
| $Sa_{avg,lower}(T) = 2.13g$ , $Sa_{avg,upper}(T) = 0.54g$                  | $Sa_{avg}(T) = 0.22g$  |
| $H(Sa_{avg,lower}(T)) = 6.81 \times 10^{-6}$ ,                             | $H(Sa_{avg}(T)) = 2.97 \times 10^{-3}$                         |
| $H(Sa_{avg,upper}(T)) = 0.36 \times 10^{-3}$ ,                             |  |
| $G_{lower} = 61.9 \times 10^{-6}$ , $G_{upper} = 0.89 \times 10^{-3}$      |  |
| $F_{lower} = 0.010$ , $F_{upper} = 0.318$                                  |  |
| $\lambda_\theta = 0.61 \times 10^{-3}$ , $T_R = 1640$ years                | $\lambda_a = 11.7 \times 10^{-3}$ , $T_R = 85$ years           |
| $\eta_{D,Direct} = 0.63g$  | $\eta_{D,Direct} = 0.24g$                                      |
| $\beta_{TOT,IM} = 0.59$  | $\beta_{TOT,IM} = 1.02$  |
| $\lambda_{\theta,Direct} = 0.63 \times 10^{-3}$ , $T_R = 1579$ years       | $\lambda_{a,Direct} = 10.5 \times 10^{-3}$ , $T_R = 95$ years  |

and direct integration approaches. As observed in Table 2, for the MPFA-sensitive component, the hazard was computed directly from the  $Sa_{avg}$  of 0.22 g. At the same time, the exact approach employs a direct integration of a capacity distribution of the component assuming a median,  $\eta_{D,Direct}$  value of 0.24 g. For what concerns the MPSD-sensitive component, following the calculations of the simplified approach, lower and upper  $Sa_{avg}$  were computed as 2.13 g and 0.54 g, which stems from the high capacity of the component and lower demands. The upper branch of the bilinear portion significantly contributes to the  $\lambda_\theta$ . In contrast, the lower branch has almost no effect, as seen from the computed values of  $F_{lower}$  and  $F_{upper}$ , which essentially act as weighting functions. This exercise shows that the MAFE of several NSEs associated with a specific damage state and located within any building can be estimated simultaneously with good accuracy and in a probabilistic manner through the simplified method described in Section 2. This is seen through accurate estimation of risk across different demand levels (MPSD, MPFA) and not just a single-point estimate for a particular damage state (e.g. collapse). These calculations can be used as a more robust means to estimate the relative safety of various NSEs and can be integrated with a classification framework described by O'Reilly and Calvi (2021).

To further understand the impact of some assumptions involved with uncertainties for each approach, the MAFE was computed for increasing demand and illustrated in Fig. 6, which are termed demand-hazard curves. To maintain consistency between the two approaches, deterministic definitions were used; therefore, the term  $\beta_{CU}$  was set to zero, while, on the other hand,  $\beta_{CR}$  was set to 0.33 and 0.60 (Table 1) for MPSD- and MPFA-sensitive components, respectively. Additionally,  $\beta_{DU}$  was assumed to be 0.3, and  $\beta_{DR}$  was computed using the MSA distributions at each IM level plotted in Fig. 5. Good matching of the demand-hazard curves was observed between both approaches at all levels of MPSD and MPFA. The vertical dashed lines corresponding to NSE mean capacities in Fig. 6 give an idea of the risk associated with the specific NSE utilised within this study. The consistency of results implies satisfactory predictions of the predictive demand-intensity models for performance quantification both in terms of MPSD and MPFA, however, more case study validations would allow the further appraisal of the models. The effective propagation of uncertainties, and high quality of fitting functions with respect to the median MSA response and MAFE computed via a direct integration method, underlines the quality of the models in capturing the response and computing risk accurately with relative ease. Therefore, the generalization of demand-intensity models for specific typologies of buildings, occupancy, and use, may help avoid cumbersome computations involving complex non-linear analyses whilst still achieving the same end result to be used in practical decision-making.

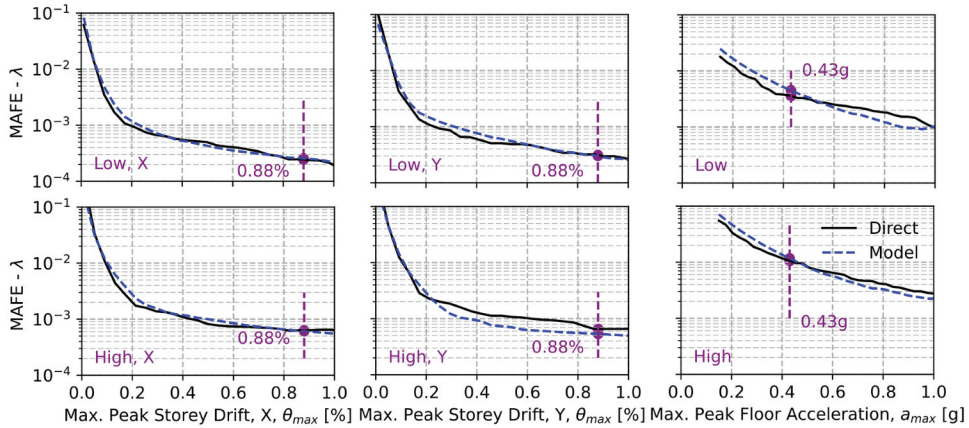


**Figure 6.** Demand–hazard curves for the case study buildings at low and high seismicity.

#### 4.2. Explicit NSE Performance Assessment

To further validate the results with respect to simplified demand–intensity models, the NSE described in Section 3.2 were explicitly modelled using OpenSees (Mazzoni et al. 2006) to investigate any possible impact on the risk outputs. It is essential to understand how the risks computed using explicit models of NSE within the structural models compare to the results of implicit models described in Section 4.1 and the simplified methods outlined in Section 2.

Having modelled the gypsum partition walls explicitly, MSA was carried out to examine the impact of explicitly considering them within the numerical models of the structure. Figure 7 provides the demand–intensity fits to the medians of peak storey drift at each storey of the building for the high seismicity location. The demand–intensity response at the fourth storey differs from other storeys due to the non-linear characteristics of the structure. Following the infill collapse at lower storeys, the PSD increases significantly with intensity at those storeys (i.e. it forms a soft-storey mechanism), while the PSD at the highest storey remains effectively unaffected. Good fitting is noted, and the resulting fitting parameters are used to carry out MAFE calculations similar to the ones described in Table 2. Additionally, it is evident that the NSE's 0.88% median capacity is not being exceeded much in the upper two storeys of the building. This indicates structure's drift demand saturating at these higher storeys, which translates to very low values of exceedance rates when computing MAFE.

Again, MSA was carried out with the acceleration-sensitive component explicitly modelled, and the median demand–intensity model fit is given in Fig. 8. Good matching of MAFeS computed via both approaches was obtained, that is  $10.2 \times 10^{-3}$  and  $10.0 \times 10^{-3}$  following the simplified demand–intensity and direct integration methods, respectively.

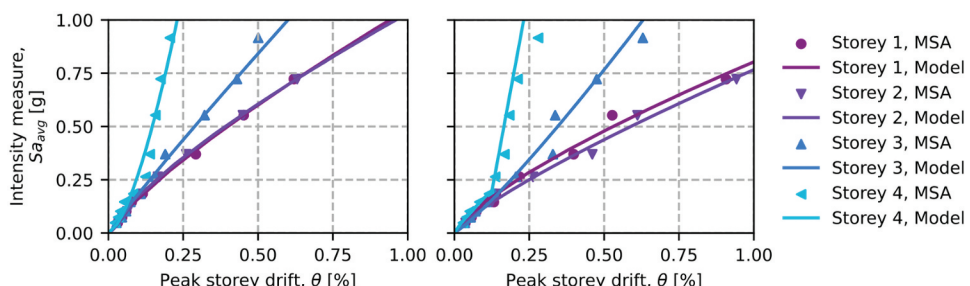


**Figure 7.** demand–intensity models of MSA results in the (left) X-direction and (right) Y-direction for the high seismicity site with gypsum partitions explicitly modelled.

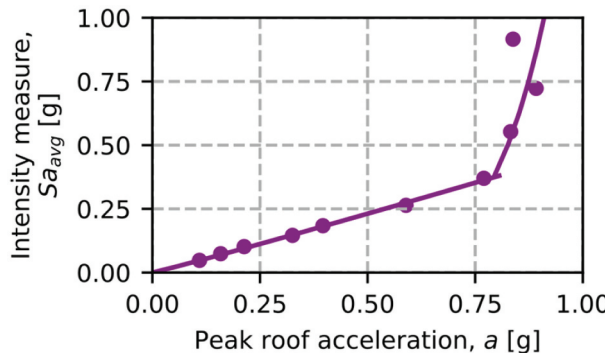


**Figure 8.** demand–intensity models of MSA results for the high seismicity site with a PFA-sensitive component explicitly modelled.

**Table 3.** Mafes computed using the fitting models and the direct integration approach for the high seismicity site with NSE implicitly and explicitly modelled.

| Direction | Storey – EDP | Explicit modelling, $\times 10^{-3}$ |        | Implicit modelling, $\times 10^{-3}$ |        |
|-----------|--------------|--------------------------------------|--------|--------------------------------------|--------|
|           |              | Simplified                           | Direct | Simplified                           | Direct |
| X         | MPSD         | 0.38                                 | 0.36   | 0.61                                 | 0.63   |
| Y         | MPSD         | 0.52                                 | 0.43   | 0.54                                 | 0.49   |
| -         | 4 – PFA      | 10.20                                | 10.00  | 7.46                                 | 6.71   |

The MAE<sub>s</sub> computed through implicit and explicit modelling are summarised in Table 3. MPSD was used as the EDP for the drift-sensitive NSE, while peak roof acceleration was used for the acceleration-sensitive NSE, as the latter was located only on the roof. Tiny variations are observed indicating good performance of implicit models even in the absence of NSE in the numerical models. Additionally, the values attained through the demand–intensity models using the simplified calculations described in Section 2 are not far off from the actual values computed through the direct integration method of the MSA results with the seismic hazard. This highlights the ability of the simplified models to capture the performance of the structure and consequently the NSE in terms of MAE without the need of running extensive NLTHA provided that the demand–intensity model fitting parameters,  $m$  and  $b$ , are known. It also goes to show that with respect to what may be considered the most accurate computation of MAE in each case (direct integration), the level of discrepancy induced by using simplified demand–intensity models is somewhat on par with the results obtained when considering the implicit numerical model results. Given the consistency of results independent of modelling type, *i.e.*, explicit and implicit, and type of NSE considered, and with the availability of  $m$  and  $b$  demand–intensity model fitting parameters, results may be leveraged to construct simplified models applicable to a large variety of buildings. Therefore, to further generalise the models and increase their availability, ML algorithms may be employed to generate models depending on building typology, occupancy, and usage and are outlined in the next section.

## 5. Algorithmic Predictions of Demand–Intensity Models

### 5.1. Methodology

Since Section 4 shows the usefulness of demand–intensity models for assessing seismic risk, this section aims to explore the training and prediction of such models with reasonable accuracy via ML methods. While the problem statement could be limited to the direct estimation of risk as the primary dependent variable, which would further simplify the ML models, an additional variable associated with the vulnerability of the NSE would need to be defined as input. Instead, estimating demand–intensity models allows convenient flexibility in its application to any type of NSE and is not limited to a specific vulnerability

function. Relationships among various variables of the building characteristics and its subsequent seismic behaviour are the desired output. In essence, the analytical problem is the estimation of  $m$  and  $b$  fitting parameters depending on building characteristics, site hazard conditions, and seismic design level. The fitting parameters have been described in [Section 2](#) and they describe the building's seismic behaviour up to collapse. Therefore, significant accuracy is not the study's goal, but rather to understand the importance and effects of variables generally known before design and assessment on the demand–intensity models or dependent variables. Several ML methods were applied to establish demand–intensity models of infilled RC buildings based on results attained via the same MSA approach outlined in [Section 2](#).

For a quick estimation of building performance in terms of demand–intensity models depending on their characteristics, a more complete dataset of infilled buildings was adapted from Nafeh and O'Reilly ([2022](#)). The dataset consisted of 35 buildings following two design eras and three site locations amounting to 210 unique data points. The key variables of the dataset include the period of construction associated with design practice, consideration of gravity and lateral load-bearing structural system, material property variations, type of occupancy and usage, building height, elevation, and plan configuration. Additionally, span distributions and spacing, compartmentalisation of living space are varied within the archetypes. Half of the building dataset consists of buildings designed before the introduction of modern seismic provisions around the 1970s in Italy, where the buildings were designed to resist gravity loads only with no ductile detailing or capacity design principles. The other half of the building dataset includes buildings of the mid-1970s and 1980s designed using an equivalent lateral force method. Those buildings followed similar design directives as the case study buildings outlined in [Section 3.1](#). The buildings were analysed via MSA, and the results were post-processed to obtain demand–intensity models. The dataset was halved depending on the EDP categorisation (210 structural models, 210 for each EDP), as two sets of ML models will be trained depending on the type of EDP.

The ML application framework for demand–intensity model prediction includes the following steps: (1) definition of independent and dependent variables determined by EDP categorisation; (2) splitting of the entire dataset into training and testing sets; (3) creation of feature engineering pipelines; (4) adaption of k-fold cross-validation (CV) to maximise the use of available data for training and validating the models; (5) selection of ML modelling approaches; (6) best performing predictive model selection based on validation metrics; (7) and interpretation of results through feature importance assessment and demand–intensity model fitting parameters' predictions. The entire flowchart is provided in [Fig. 9](#), and the details for each step will be provided in the following text.

A multi-variate multiple regression-based approach was used within the study given the multiple independent variables and multiple dependent variables in terms of lower, upper  $b$  and  $m$  values, within the employed ML models. The first step of the approach utilised herein defines the independent and dependent variables following step (1) of [Fig. 9](#). The independent variables include building and hazard characteristics: design, indicating whether the building was designed under seismic and gravity load conditions (SSD), or gravity only (GLD); site location for low, medium and high seismicity; the number of storeys ranging from 2 to 6; building global dimensions; variables describing the infill distribution along both primary directions of the building involving three strength definitions ([Hak et al. 2012](#)); irregularity indicating whether stiffness irregularities exist along the height of the building, and plan area. Additional variables considered within the ML models provide more insight into structural behaviour and need preliminary assessment in terms of eigenvalue and static pushover analysis: the secant to peak strength periods in both directions; and a limit variable of IM (for MPFA training) and EDP (for MPSD training) in both directions, which are necessary only for bilinear demand–intensity fitting functions. The limit variable may be assumed based on physical reasoning associated with a specific structural systems' response (e.g. structural yielding or masonry infill collapse), that can be pre-established through simple static pushover analysis ([O'Reilly and Monteiro 2019](#)). Fundamentally, the training algorithm attempted the prediction of 4 and 8 dependent variables associated with MPFA and MPSD EDPs, respectively. The range of values for the features are listed in [Table 4](#), which correspond to the applicable limits of ML models developed herein. Variables

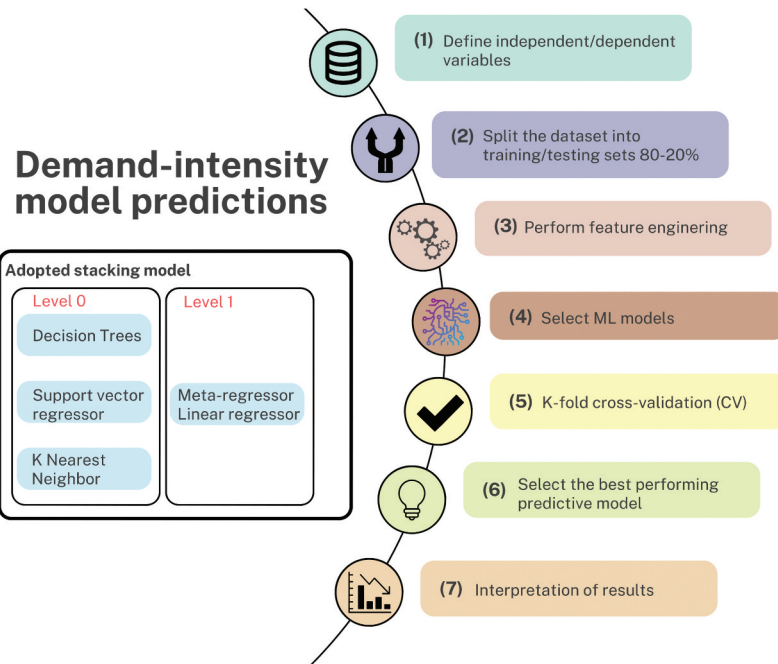


Figure 9. Flowchart of the ML application and stacking model used.

Table 4. Statistical information of numerical independent and dependent features.

| Feature                     | Unit           | Min.      | Max.        | Mean      | St. D.    | Type        |
|-----------------------------|----------------|-----------|-------------|-----------|-----------|-------------|
| Area                        | m <sup>2</sup> | 124.2     | 207.9       | 175.4     | 24.8      | Independent |
| Weak infill lengths         | m              | 0.0       | 30.8        | 11.3      | 12.6      | Independent |
| Medium infill lengths       | m              | 42.6      | 63.6        | 55.9      | 6.5       | Independent |
| Strong infill lengths       | m              | 10.0      | 18.4        | 13.4      | 2.8       | Independent |
| Periods                     | s              | 0.29      | 1.12        | 0.60      | 0.19      | Independent |
| Limit for MPFA              | g              | 0.04      | 0.93        | 0.34      | 0.28      | Independent |
| Limit for MPSD              | %              | 0.07      | 0.62        | 0.16      | 0.05      | Independent |
| $m_{low,MPFA}/m_{low,MPSD}$ | –              | 0.05/0.16 | 4.20/1.34   | 1.48/0.48 | 0.61/0.19 | Dependent   |
| $b_{low,MPFA}/b_{low,MPSD}$ | –              | 0.42/0.38 | 1.35/1.31   | 0.80/0.88 | 0.15/0.12 | Dependent   |
| $m_{up,MPFA}/m_{up,MPSD}$   | –              | 0.71/0.18 | 2.47/30.00* | 1.35/5.61 | 0.37/4.62 | Dependent   |
| $b_{up,MPFA}/b_{up,MPSD}$   | –              | 0.20/0.30 | 2.50/6.98*  | 0.72/2.61 | 0.29/0.78 | Dependent   |

\*very high value signifying saturation of response.

with homogeneous distributions are not provided (e.g. three sites are equally represented). As observed, some dependent variables have enormous values, which are indicators of structural response saturation, where the demand–intensity curve plateaus. It is important to note that even though the upper values of  $m$  are higher than the lower values for the MPFA cases, this is primarily due to having a significant number of empty values due to linear fits.

In step (2) of Fig. 9, the dataset is split into training and testing sets. As a general approach in ML, the best results were shown to have been attained when the dataset was split between 70% and 80% training and 30–20% testing sets, respectively. Therefore, this study adopted an 80–20% ratio of training and testing sets.

With the dataset pre-processing steps outlined, feature engineering pipelines were created for further model training (step (3) of Fig. 9). Pipelines were used to apply sequential transformations on the independent variables for joint cross-validation. The use of pipelines aids in avoiding data leakage during the pre-processing steps. Therefore, the trained model may be safely used for unseen test and validation datasets. Based on variable types, feature engineering can be broken down into

three categories: adding, removing, and changing. New variables might be necessary to provide more insight, while others might be dropped, leading to a reduction of data dimensionality. The independent dataset was scaled between 0 and 1 using Eq. (9), although other methods, such as standard deviation scaling, could have been employed.

$$x' = \frac{x - \min(x)}{\max(x) - \min(x)} \quad (9)$$

where,  $x$  is the original value and  $x'$  is the normalised value. As a result, the dataset has smaller standard deviations suppressing the effect of outliers. Additionally, this is done as some ML algorithms may fail or take more iterations to complete the training because of convergence issues.

The Lmit variable corresponds to  $s_{lim}$  and  $\theta_{lim}$  for MPFA and MPSD demand–intensity models, respectively. It was recorded when a bilinear demand–intensity model was utilised to characterise the performance of the building in either of its directions. In the case of linear fits, the variable was left empty, essentially meaning that no upper dependent variables were provided. To capture whether demand–intensity models were linear or bilinear, a new variable indicator was added (Fitting variable). Additionally, for linear fits no upper fitting parameters were captured; therefore, it was decided to impute them with the lower branch of fitting parameters since no variation was expected. Even though a new independent variable was added based on the limit feature, the numeric values of the limit feature carry some level of importance, indicating a point after which the fit changed its gradient. Therefore, to avoid dismissing the entire descriptor, it was decided to use an imputation for missing values through a random sampling approach based on the distribution of existing values. This approach was selected to preserve the variable distribution shape (Fig. 10). For categorical variables, dummy variables were created to distinguish between variable subgroups within design and site. Dummy variables enable the use of a single regression equation to represent multiple groups, as most ML algorithms do not work with categorical variables. Essentially, a site variable will be transformed into  $k - 1$  variables, where  $k$  represents the number of unique values.

To avoid multicollinearity, which is the occurrence of high intercorrelations among two or more independent variables, a correlation matrix is plotted in Fig. 11(left). To avoid the multicollinearity issue, where having all three sites present in the data result in less reliable statistical inferences, the dummy variable associated with L'Aquila was dropped. Additionally, as expected, there is high correlation between Period variables and the number of storeys (Crowley et al. 2017). Therefore, it was decided to omit the Period variables, as they bring no additional information to the training model.

To highlight the relationship among dependent variables, a correlation matrix is displayed in Fig. 11(right). As observed, there is a strong relationship between the  $m$  and  $b$  variables corresponding to the same EDP and direction. However, a strong relationship may be observed between the  $m$  and

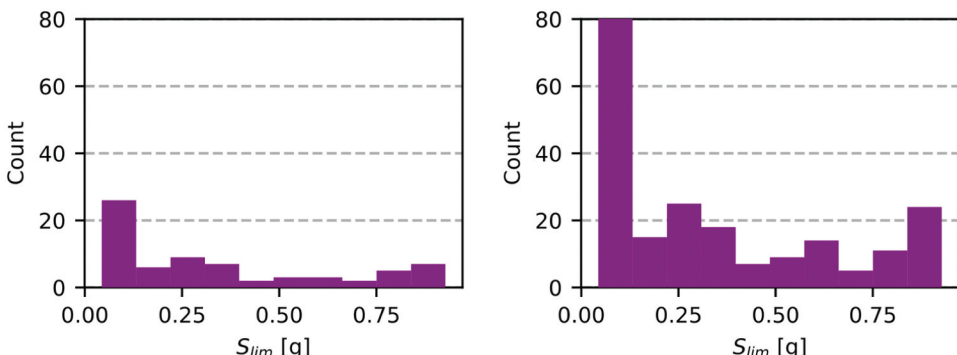


**Figure 10.** Limit feature distribution associated with MPFA before (left) and after (right) imputation.

$b$  variables of different EDP values, highlighting the importance of considering them during the training of the models. While considering one pair of  $m$  and  $b$  parameters could be of great importance in predicting another set of parameters, it is highly unlikely to have data on those parameters before the application of the models. Therefore, this study did not consider the relationship between different dependent variables. To visualise the distribution of the fitting parameters, as seen in Fig. 12, the majority of  $m$  and  $b$  values of the lower branch are in a range between 0.5–1.0 and 0.2–1.2, respectively. However, the  $m$  and  $b$  values of the upper branch associated with MPSD are plotted to signify a more significant dispersion of values between 0.5–6.0 and 0.2–30, respectively. First clues regarding outliers may be gathered from those plots, even though larger values possibly indicate the saturation of demand-intensity models. Given the quantitative disadvantage of those, it is generally advisable to avoid them for imbalance issues.

Several parametric and non-parametric ML (assuming non-functional form) models were employed in this study using multiple multivariate regression to predict the multiple continuous output variables (step (4) of Fig. 9). Parametric approaches such as linear and ridge regression work well when a relationship between independent and dependent variables is reasonably linear. At the same time, decision tree, random forest, and boosting methods are stronger when complex non-linear relationships are expected between the independent and dependent variables. Several approaches were utilized within the study: parametric approaches such as multiple multivariate ridge and lasso regression, non-parametric approaches such as DT, KNN, SVR and XGBoost (Chen and Guestrin 2016). Additionally, a stacked generalization model (Wolpert 1992) combined the predictions from multiple ML models on the dataset. XGBoost and stacked generalisation are ensemble methods where new models learn how to best combine predictions from numerous previous models via a meta-regressor (Fig. 9) which is not very dissimilar to the use of logic trees in PSHA for example. Unlike bagging (produces weak learners in parallel through Bootstrap

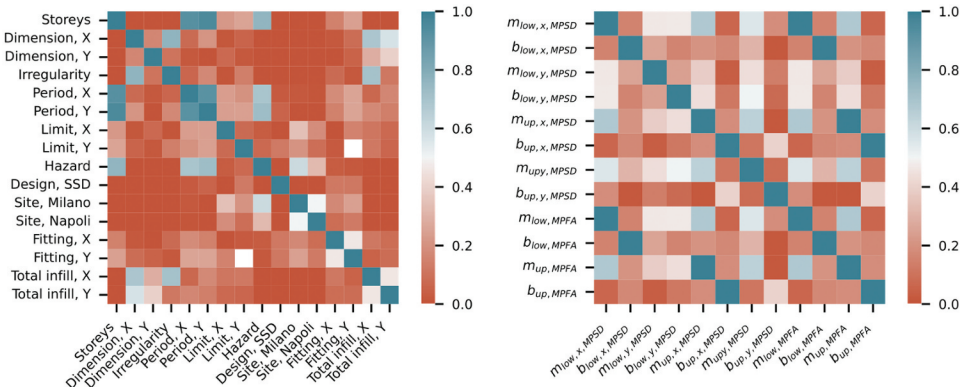


Figure 11. Correlation matrix of independent variables (left) and dependent variables (right).

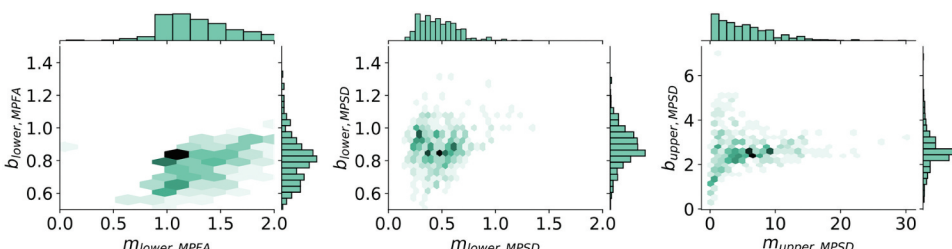


Figure 12. Distribution of demand-intensity model fitting parameters associated with MPSD and MPFA.

sampling) and boosting (produces weak learners sequentially), stacking may be used to combine models of different types.

Hyper-parameter tuning was performed on the training set via a grid search algorithm using a repeated k-fold CV (step (5) of Fig. 9). Generally, ten folds are recommended in the literature (Kuhn and Johnson 2018). A repeated k-fold CV provided ways to improve the estimated performance of an ML model. It involved a procedure where the mean results were reported across all folds and runs. This is a powerful tool for small datasets, appropriate for this study. The selected CV procedure divides the dataset into k non-overlapping folds. Each fold can be used as a held back validation set, while the rest are used as a training dataset. A total of  $k$  models were fit and evaluated on the  $k$  hold-out validation sets, and finally, the mean performance was computed. Additionally, as already outlined earlier, before subdividing the dataset into k folds, 20% of the original dataset was randomly separated for final testing and prediction. The calibrated ensemble models via hyperparameter tuning include a number of boosting rounds or trees (weak learners) to build, early stopping rounds (stops training if performance did not improve for certain rounds), maximum depth of a tree, minimum weight required the creation of a new node in the tree, fraction of observations and fraction of variables to use, and the learning rate. All combinations of those parameters were used iteratively through a grid search algorithm to train the model and apply the  $k$ -fold CV to find the best performance.

The goodness-of-fit test was implemented based on mean absolute error (MAE) (Eq. (10)) and the coefficient of determination or R-squared ( $R^2$ ) score (Eq. (11)) for ranking the training models, and for final best performing predictive model selection (step (6) of Fig. 9). MAE indicates the relative error between predicted and observed values with the lower value being better.  $R^2$  is a statistical entity representing the proportion of the variance of a dependent variable that is explained by the independent variables in a regression model. A 0%  $R^2$  value does not explain the variation in the dependent variable around its mean. On the contrary, 100% represents a model that perfectly explains the variation in the dependent variable around its mean.

$$MAE = \frac{\sum_{i=1}^n |y_i - \hat{y}_i|}{n} \quad (10)$$

$$R^2 = 1 - \frac{\sum_{i=1}^n (y_i - \hat{y}_i)^2}{\sum_{i=1}^n (y_i - \bar{y})^2} \quad (11)$$

where  $y_i$  is the  $i$ th observed value,  $\hat{y}_i$  is the  $i$ th predicted value, and  $\bar{y}$  is the mean value of n data points.

## 5.2. Results and Discussion

The demand-intensity models associated with MPSD and MPFA of the infilled RC buildings were predicted using the ML models following the procedures described in Section 5.1 (step (7) of Fig. 9). The hyper-parameters of the applied models were optimised through the same grid search method and a 10-fold CV. Grid search was applied, where a grid of hyperparameter values was chosen and validation metrics were evaluated. The XGBoost and stacked generalization methods (stacking) demonstrated the best performance compared to the methods using a single predictive algorithm determined from the MAE and  $R^2$  values in Fig. 13. As observed, the XGBoost shows higher  $R^2$  on the test set than the stacking model, while the MAE are on a relatively similar level. Therefore, the remaining part of the study concentrates on XGBoost. The calibrated hyper-parameters of the XGBoost algorithm are summarised in Table 5.

Feature importance analysis was conducted to understand the complex relationships between independent and dependent variables. Following the expedited nature and overall objective of the approach being studied, the feature importance analysis could be of general interest to designers and stakeholders. For this reason, SHAP was used to explain the outputs of the ML models employed (Lundberg and Lee 2017). SHAP can provide impact and correlation of independent variables, as well

as their importance for predictions. As seen in Fig. 14, for all dependent variables, the hazard is the most important independent variable for the predictions, followed by the number of storeys and a design type. As already visualised in Fig. 5, with aggressive hazard associated with the high seismicity region and consequent ground motions selected, the seismic response of the buildings is expected to differ, resulting in different  $m$  and  $b$  fitting parameters with respect to the lower hazard site. Kohrangi, Vamvatsikos, and Bazzurro (2017) among others, has also demonstrated the importance of site dependence of ground motion selection on building fragility assessment, followed by proposed formulations to account for multiple sites in hazard disaggregation. In contrast, the irregularity, the archetype configuration related to the layout of the building, and the infills have lower effects on the estimation of the fitting parameters relative to the more critical variables. This helps to build some perspective on further improvement of the ML algorithms and understanding which variables are essential in the prediction of building performance until collapse. One observation may be that given the relative importance of site hazard, future work ought to consider data from multiple sites with varying seismic hazard levels and possible tectonic environments, as investigated by Fox and O'Reilly (2022), for example, in order to have a more robust and accurate ML model.

As seen in Section 2.2, due to saturation of EDP with increasing intensity because of structural yielding or masonry infills collapsing, a bilinear demand–intensity relationship is more suitable than a linear one. Therefore, when making predictions, another important predictor is the Fitting variable (Fig. 14), which is a Boolean indicator of bilinear or linear demand–intensity relationship. Predictions of the upper branch of a bilinear fitting function are obligatory only in the case of a *true* Fitting feature

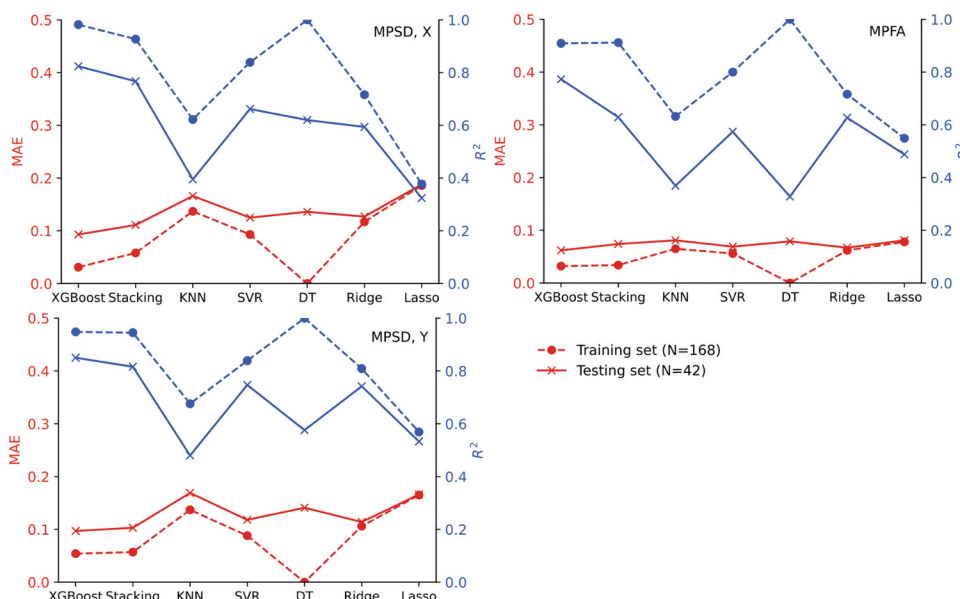


Figure 13. Training and testing MAE and  $R^2$  values of the applied ML algorithms.

Table 5. Hyper-parameters of the XGBoost method.

| Parameter                           | MPFA | MPSD, X | MPSD, Y |
|-------------------------------------|------|---------|---------|
| Number of trees to build            | 43   | 164     | 157     |
| Maximum depth of tree               | 3    | 6       | 4       |
| Minimum weight to create a new node | 8    | 11      | 10      |
| Subsample of observations to use    | 100% | 100%    | 90%     |
| Subsample of features to use        | 100% | 100%    | 70%     |
| Learning rate                       | 0.3  | 0.1     | 0.05    |

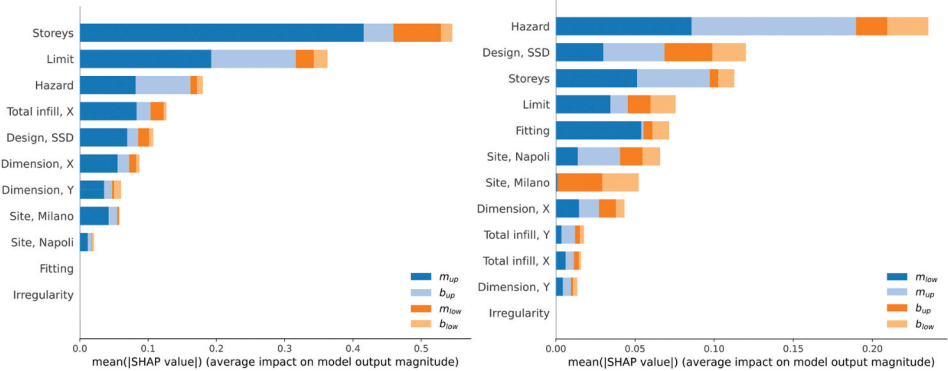
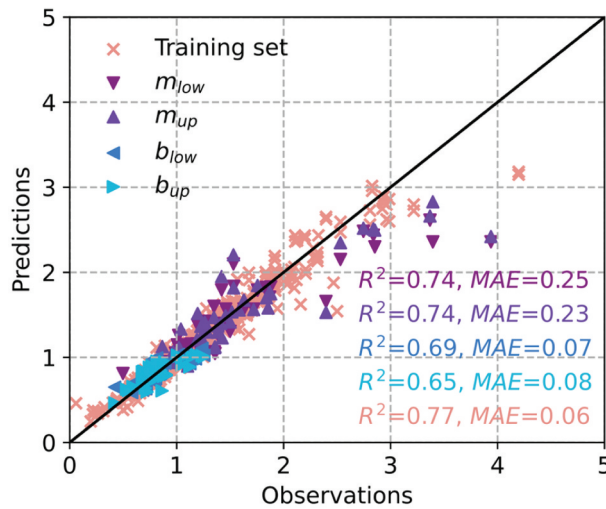


Figure 14. Feature importance analysis results: (left) MPSD in the X direction, (right) MPFA.

value. However, within this study, the imputation of values was carried out for the upper branch, resulting in predictions which are less than ideal for the upper branch. This indicates a necessity of a larger dataset where the bilinear relationship is more desired, and therefore, due to a significant portion of missing data from the original dataset related to upper branch fitting parameters associated with linear demand–intensity models, only the accuracy of lower branch fitting parameters is visualised in Fig. 15. This is a limitation of an employed approach because of limited data, however, has no influence on the lower branch, as the lower branch parameters are predicted independently from the upper branch. It is foreseen that with increase of data points, the model could be enhanced to capture the behaviour of non-linear systems with higher accuracy and introduce less bias due to imputation of missing values. Additionally, as seen in Fig. 14(left), the fitting variable carries no importance due to having predominantly bilinear models associated with MPSD, which is not the case in Fig. 14(right) for MPFA cases, where the quantity of linear or bilinear fits is similar. Most of the test data points lie approximately on a straight line ( $y = \hat{y}$ ). In general, relatively close  $R^2$  scores are observed between the training and testing set results indicating low variance (i.e. no overfitting); however, some improvements may be made, as suggested earlier with regard to improving the dataset and the MSA results.

To what regards to the prediction of demand–intensity fitting parameters pertaining to MPSD, Fig. 16 plots the predictions and accuracy metrics in X and Y directions. Relatively good matching and high accuracy is obtained, however some imperfections are noted. Even though the  $R^2$  scores associated with the lower branch  $b$  values are low, meaning that the variance of the  $b$  value is not well explained, the very low corresponding MAE suggests satisfactory predictions. In contrast the  $R^2$  score of the upper branch fitting parameters is quite high, however, the MAEs are high as well in comparison with the lower branch fitting parameter predictions. While, the accuracy seems low, the actual values of upper branch fitting parameters are higher in contrast to the lower branch as observed in Fig. 12, suggesting once again satisfactory performance of the ML models.

To understand how the ML predictions transfer to actual predicted demand–intensity fitting functions, Fig. 17(left) plots the demand–intensity models estimated using the simplified approach described in Section 2.1 and the ML algorithmic results described here. The results indicate very similar demand–intensity curves, emphasizing the ML predictions’ accuracy in practical terms. Moreover, as expected, given the relatively straight shape of the curves in logspace, the imputation of limit variable (discussed in Section 5.1) did not have a biasing effect on the results, as the upper branch prediction matched the observations with relatively good accuracy. Additionally, the MAE were computed for the MPFA-sensitive NSE of Table 1 following the predicted relationships and plotted in Fig. 17(right), where excellent matching is observed. This speaks to the adequacy of simplified methods in capturing complex analysis results such as MSA with relative ease without requiring extensive numerical analyses.



**Figure 15.** Observed and predicted values of demand–intensity model fitting parameters associated with MPFA.

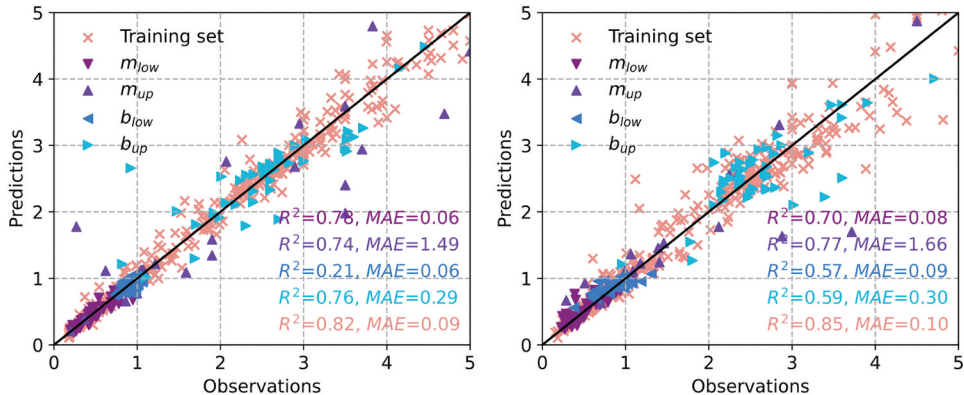


**Figure 16.** Observed and predicted values of demand–intensity mode-fitting parameters associated with MPSD: (left) X direction, (right) Y direction.

Similarly, for the MPSD-sensitive NSE of Table 1 in the X-direction of the building, Fig. 18(left) demonstrates the demand–intensity models computed and Fig. 18(right) plots the corresponding MAEs. Following the predicted relationships, it can be seen that good matching is attained despite slightly subpar matching by the ML model-based estimate at higher MPSD values. The main reason for this was because of higher dispersion of values as a direct result of the saturated response of the building at higher MPSD values as illustrated in Fig. 12.

The study described here intended to act as a steppingstone for more large-scale analysis and training of models with higher accuracy and quality. It is envisioned to be an important tool for quick estimation of building performance during design and after earthquakes for practitioners, researchers, and insurance companies. Its integration within national seismic design codes for estimating the risk associated with structural performance and NSEs located in the building premises similar to the calculations demonstrated in Section 4 is also possible. Future research should involve the ease of integration of larger datasets for further training and transfer learning. The latter involves using already trained models for use in similar problems, for example, involving other building typologies, or extending to newer datasets. For example, Feng, Zhou, and Dong (2019) demonstrated how pre-trained deep neural networks (DNNs)

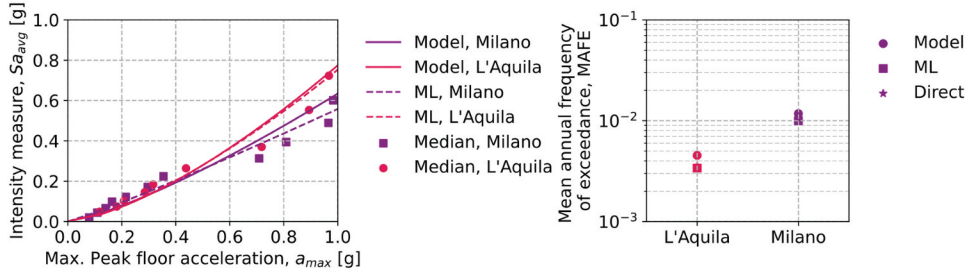


**Figure 17.** demand–intensity models of the case study building of Section 3.1 estimated via simplified approaches and ML predictions on the median response of MSA in terms of MPFA (left), and the MAFEs compared following the three approaches utilised (right).

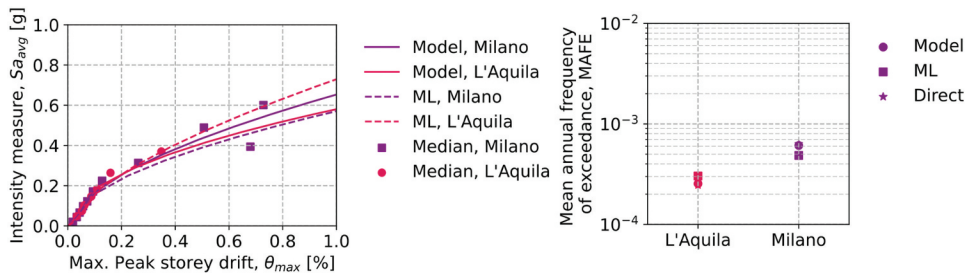


**Figure 18.** demand–intensity models of the case study building of Section 3.1 estimated via simplified approaches and ML predictions on the median response of MSA in terms of MPSD in the X direction (left), and the MAFEs compared following the three approaches utilised (right).

perform significantly better than training DNNs by conventional methods on a small dataset. Therefore, the goal is to open a space for the ease of integration of new datasets, which could potentially result in change or the addition of other objectives as well as augmented quality and accuracy.

## 6. Summary and Conclusions

Ensuring collapse safety and avoiding loss of life is imperative in the earthquake engineering community. Nonetheless, losses incurred by damaged non-structural elements (NSE) constituting the significant share of entire losses following earthquakes drove the scientific community to advance methodologies for risk-oriented design and assessment of NSEs. demand–intensity models developed for structural elements have been adapted to calculate risks associated with the NSEs. In this study, demand–intensity models were applied to quantify risks associated with reinforced concrete (RC) buildings with masonry infills. Two numerical modelling techniques were utilized:

- (1) Implicit numerical modelling, where the structural model was created without consideration of NSE properties, and NSE performance was inferred from the structural response;
- (2) Explicit numerical modelling, where the NSE models were directly incorporated into the structural model, assessed the coupled response. The models were created using both a peak floor acceleration (PFA) and peak storey drift (PSD) sensitive NSE.

Both approaches were validated with respect to the direct integration method used in calculating mean annual frequency of exceedance (MAFE) of a given limit state using multiple stripe analysis results in terms of PSD and PFA. The demand–intensity models were appraised via machine learning (ML)



regression models trained on a dataset of RC buildings with masonry infills to further expedite and simplify the assessment techniques. The regression models were employed to predict the fitting parameters of linear and bilinear demand–intensity models using building characteristics typically available before structural design or assessment. That is, layout configuration, number of storeys, design era, site location and associated seismic hazard, availability of infill walls, and stiffness irregularity. The models were limited to in-plane failure mechanisms of infill walls. The pretrained ML models envisage their use for a portfolio of buildings depending on their usage, typology, and occupancy.

Based on this investigation, several points can be noted:

- demand–intensity models were fitted to the multiple stripe analysis (MSA) median maximum PSD and maximum PFA results of the case study buildings. Both implicit and explicit numerical modelling approaches were fitted, and good conformance compared to the direct integration of MSA results was obtained. The MAFEs computed following the demand–intensity models associated with maximum PSD were in the range of  $0.38\text{--}0.52 \times 10^{-3}$  and  $0.54\text{--}0.61 \times 10^{-3}$  for the implicit and explicit modelling approaches, respectively. The MAFEs associated with maximum PFA computed for implicit and explicit models were around  $7\text{--}10 \times 10^{-3}$ , respectively.
- Several multivariate ML regression models were employed on a dataset containing 35 RC buildings with masonry infills assessed via MSA in terms of both maximum PSD and PFA. XGBoost demonstrated the highest  $R^2$  and lowest mean absolute error (MAE) on the test set attained via hyper-parameter cross-validation compared to the other models and was therefore selected as the final best performing predictive model. A  $R^2$  of the model was 0.84 and 0.77, while MAE was 0.09 and 0.06 associated with maximum PSD and PFA, respectively.
- Feature importance analysis was carried out using SHapley Additive exPlanations (SHAP), where hazard, number of storeys and design type were highlighted as the most important features for fitting parameter prediction.
- demand–intensity models predicted via XGBoost, and subsequent MAFEs computed for both site locations pertinent to the case study building were very similar to the observed demand–intensity models and the direct integration method previously examined.

Several limitations are noted, in specific, with regard to insufficient data, which constrain the training ability as well as the quality. Additionally, the dataset is randomly split into a training set and a testing set with a 80%–20% proportion, where the training set was further split using a Repeated k-fold cross-validation (Mosteller and Tukey 1968) due to limited data. The limitation of data is a constraint; however, reasonable accuracy at this stage highlights the importance of ML models for quick estimation and further improvement with data availability. The ML models are envisaged to be used for any RC building with masonry infills for quick performance estimation without any complex numerical analysis using only limited information regarding the building that was utilised within this study. Thus, the pre-trained ML models could potentially be used for structural and non-structural risk assessment for such buildings where little detailed information is available. The pre-trained XGBoost models as well as the dataset developed are freely available at Shahnazaryan and O'Reilly (2022).

## Disclosure statement

No potential conflict of interest was reported by the author(s).

## Funding

The work presented in this paper has been developed within the framework of the project “Dipartimenti di Eccellenza”, funded by the Italian Ministry of Education, University and Research at IUSS Pavia.

## ORCID

Davit Shahnazaryan  <http://orcid.org/0000-0002-0529-5763>  
 Gerard J. O'Reilly  <http://orcid.org/0000-0001-5497-030X>

## References

- Ancheta, T. D., R. B. Darragh, J. P. Stewart, E. Seyhan, W. J. Silva, B. S. J. Chiou, K. E. Wooddell, R. W. Graves, A. R. Kottke, D. M. Boore, and Kishida T. 2014. "NGA-West2 Database." *Earthquake Spectra* 30 (3): 989–1005. <https://doi.org/10.1193/070913EQS197M>.
- Aschheim, M., and E. F. Black. 2000. "Yield Point Spectra for Seismic Design and Rehabilitation." *Earthquake Spectra* 16 (2): 317–335. <https://doi.org/10.1193/1.1586115>.
- Baker, J. W. 2011. "Conditional Mean Spectrum: Tool for Ground-Motion Selection." *Journal of Structural Engineering* 137 (3): 322–331. [https://doi.org/10.1061/\(ASCE\)ST.1943-541X.0000215](https://doi.org/10.1061/(ASCE)ST.1943-541X.0000215).
- Chen, T., and C. Guestrin. 2016. "XGBoost: A Scalable Tree Boosting System." *Proceedings of the ACM SIGKDD International Conference on Knowledge Discovery and Data Mining* 13–17-Augu:785–794. <https://doi.org/10.1145/2939672.2939785>.
- Conte, J. P., A. J. Durrani, and R. O. Shelton. 1994. "Seismic Response Modeling of Multi-Story Buildings Using Neural Networks." *Journal of Intelligent Material Systems and Structures* 5 (3): 392–402. <https://doi.org/10.1177/1045389X9400500312>.
- Cornell, C. A. 1996. "Calculating Building Seismic Performance Reliability: A Basis for Multi-Level Design Norms." In *11th World Conference on Earthquake Engineering*, Acapulco, Mexico, 23–28 June 1996.
- Cornell, C. A., F. Jalayer, R. O. Hamburger, and D. A. Foutch. 2002. "Probabilistic Basis for 2000 SAC Federal Emergency Agency Steel Moment Frame Guidelines." *Journal of Structural Engineering* 128 (4): 526–533. [https://doi.org/10.1061/\(ASCE\)0733-9445](https://doi.org/10.1061/(ASCE)0733-9445).
- Cosenza, E., C. Del Vecchio, M. Di Ludovico, M. Dolce, C. Moroni, A. Prota, and E. Renzi. 2018. "The Italian Guidelines for Seismic Risk Classification of Constructions: Technical Principles and Validation." *Bulletin of Earthquake Engineering* 16 (12): 5905–5935. <https://doi.org/10.1007/s10518-018-0431-8>
- Crowley, H., B. Polidoro, R. Pinho, and J. van Elk. 2017. "Framework for Developing Fragility and Consequence Models for Local Personal Risk." *Earthquake Spectra* 33 (4): 1325–1345. <https://doi.org/10.1193/083116EQS140M>.
- Dávalos, H., and E. Miranda. 2019. "Evaluation of the Scaling Factor Bias Influence on the Probability of Collapse Using SA(T1) as the Intensity Measure." *Earthquake Spectra* 35 (2): 679–702. <https://doi.org/10.1193/011018EQS007M>.
- Eads, L., E. Miranda, and D. G. Lignos. 2015. "Average Spectral Acceleration as an Intensity Measure for Collapse Risk Assessment." *Earthquake Engineering & Structural Dynamics* 44 (12): 2057–2073. <https://doi.org/10.1002/eqe.2575>.
- FEMA. 2012. *FEMA P58-3. Seismic Performance Assessment of Buildings Volume 3 - Performance Assessment Calculation Tool (PACT)*. Washington, D.C: Federal Emergency Management Agency.
- Feng, S., H. Zhou, and H. Dong. 2019. "Using Deep Neural Network with Small Dataset to Predict Material Defects." *Materials and Design* 162:300–310. <https://doi.org/10.1016/j.matdes.2018.11.060>.
- Ferrario, E., N. Pedroni, E. Zio, and F. Lopez-Caballero. 2017. "Bootstrapped Artificial Neural Networks for the Seismic Analysis of Structural Systems." *Structural Safety* 67 (November): 70–84. <https://doi.org/10.1016/j.strusafe.2017.03.003>.
- Filiatrault, A., and T. Sullivan. 2014. "Performance-Based Seismic Design of Nonstructural Building Components: The Next Frontier of Earthquake Engineering." *Earthquake Engineering and Engineering Vibration* 13 (1): 17–46. <https://doi.org/10.1007/s11803-014-0238-9>.
- Filiatrault, A., C. M. Uang, B. Folz, C. Christopoulos and K. Gatto. 2001. *Reconnaissance Report of the February 28, 2001 Nisqually (Seattle-Olympia) Earthquake*. San Diego, La Jolla, CA.
- Fox, M. J., and G. J. O'Reilly. 2022. "Exploring the Site Dependency of Fragility Functions in Risk-Targeted Design." *Earthquake Engineering & Structural Dynamics* 52 (13): 4148–4163. <https://doi.org/10.1002/eqe.3783>.
- Gentile, R., and C. Galasso. 2022. "Surrogate Probabilistic Seismic Demand Modelling of Inelastic Single-Degree-Of Freedom Systems for Efficient Earthquake Risk Applications." *Earthquake Engineering and Structural Dynamics* 51 (2): 492–511. <https://doi.org/10.1002/eqe.3576>.
- Hak, S., P. Morandi, G. Magenes, and T. J. Sullivan. 2012. "Damage Control for Clay Masonry Infills in the Design of RC Frame Structures." *Journal of Earthquake Engineering* 16 (SUPPL. 1): 1–35. <https://doi.org/10.1080/13632469.2012.670575>.
- Huang, H., and H. V. Burton. 2019. "Classification of In-Plane Failure Modes for Reinforced Concrete Frames with Infills Using Machine Learning." *Journal of Building Engineering* 25:100767. <https://doi.org/10.1016/j.jobe.2019.100767>.
- Jalayer, F. 2003. *Direct Probabilistic Seismic Analysis: Implementing Non-Linear Dynamic Assessments*. PhD thesis. Palo Alto, CA: Stanford University.



- Kohrangi, M., P. Bazzurro, D. Vamvatsikos, and A. Spillatura. 2017. "Conditional Spectrum-Based Ground Motion Record Selection Using Average Spectral Acceleration." *Earthquake Engineering & Structural Dynamics* 46 (10): 1667–1685. <https://doi.org/10.1002/eqe.2876>.
- Kohrangi, M., D. Vamvatsikos, and P. Bazzurro. 2017. "Site Dependence and Record Selection Schemes for Building Fragility and Regional Loss Assessment." *Earthquake Engineering and Structural Dynamics* 46 (10): 1625–1643. <https://doi.org/10.1002/eqe.2873>.
- Krawinkler, H., F. Zareian, R. A. Medina, and L. F. Ibarra. 2006. "Decision Support for Conceptual Performance-Based Design." *Earthquake Engineering and Structural Dynamics* 35 (1): 115–133. <https://doi.org/10.1002/eqe.536>.
- Kuhn, M., and K. Johnson. 2018. *Applied Predictive Modeling*. New York, NY: Springer.
- Lundberg, S. M., and S. I. Lee. 2017. "A Unified Approach to Interpreting Model Predictions." *Advances in Neural Information Processing Systems* 2017-Decem (Section 2): 4766–4775.
- Mazzoni, S., F. McKenna, M. H. Scott, and G. L. Fenves. 2006. *OpenSees Command Language Manual*.
- McKenna, F., M. H. Scott, and G. L. Fenves. 2010. "Nonlinear Finite-Element Analysis Software Architecture Using Object Composition." *Journal of Computing in Civil Engineering* 24 (1): 95–107. [https://doi.org/10.1061/\(asce\)cp.1943-5487.0000002](https://doi.org/10.1061/(asce)cp.1943-5487.0000002).
- Merino Vela, R. J., E. Brunesi, and R. Nascimbene. 2019. "Seismic Assessment of an Industrial Frame-Tank System: Development of Fragility Functions." *Bulletin of Earthquake Engineering* 17 (5): 2569–2602. <https://doi.org/10.1007/s10518-018-00548-2>.
- Mori, F., A. Mendicelli, M. Moscatelli, G. Romagnoli, E. Peronace, and G. Naso. 2020. "A New V s30 Map for Italy Based on the Seismic Microzonation Dataset." *Engineering Geology* 275 (March): 105745. <https://doi.org/10.1016/j.enggeo.2020.105745>.
- Mosteller, F., and J. W. Tukey. 1968. "Data Analysis, Including Statistics." In *Handbook*. Reading, MA. <https://www.bibsonomy.org/bibtex/2aa6e6f5878a7845423a226845f668e0/brefeld>.
- Nafeh, A. M. B., and G. J. O'Reilly. 2022. "Unbiased Simplified Seismic Fragility Estimation of Non-Ductile Infilled RC Structures." *Soil Dynamics and Earthquake Engineering* 157 (March): 107253. <https://doi.org/10.1016/j.soildyn.2022.107253>.
- O'Reilly, G. J. 2021. "Seismic Intensity Measures for Risk Assessment of Bridges." *Bulletin of Earthquake Engineering* 19 (9): 3671–3699. <https://doi.org/10.1007/s10518-021-01114-z>.
- O'Reilly, G. J., and G. M. Calvi. 2019. "Conceptual Seismic Design in Performance-Based Earthquake Engineering." *Earthquake Engineering & Structural Dynamics* 48 (4): 389–411. <https://doi.org/10.1002/eqe.3141>.
- O'Reilly, G. J., and G. M. Calvi. 2020. "Quantifying Seismic Risk in Structures via Simplified Demand–Intensity Models." *Bulletin of Earthquake Engineering* 18 (5): 2003–2022. <https://doi.org/10.1007/s10518-019-00776-0>.
- O'Reilly, G. J., and G. M. Calvi. 2021. "A Seismic Risk Classification Framework for Non-Structural Elements." *Bulletin of Earthquake Engineering* 19 (13): 5471–5494. <https://doi.org/10.1007/s10518-021-01177-y>.
- O'Reilly, G. J., and R. Monteiro. 2019. "Probabilistic Models for Structures with Bilinear Demand–Intensity Relationships." *Earthquake Engineering and Structural Dynamics* 48 (2): 253–268. <https://doi.org/10.1002/eqe.3135>.
- O'Reilly, G. J., D. Perrone, M. Fox, R. Monteiro, and A. Filiatrault. 2018. "Seismic Assessment and Loss Estimation of Existing School Buildings in Italy." *Engineering Structures* 168 (February): 142–162. <https://doi.org/10.1016/j.engstruct.2018.04.056>.
- Pagani, M., D. Monelli, G. Weatherill, L. Danciu, H. Crowley, Silva V, Henshaw P., Butler L, Nastasi M, Panzeri L, and M Simionato, et al. 2014. *OpenQuake Engine : An Open Hazard (And Risk) Software for the Global Earthquake Model*. <https://doi.org/10.1785/0220130087>.
- Perrone, D., P. M. Calvi, R. Nascimbene, E. C. Fischer, and G. Magliulo. 2019. "Seismic Performance of Non-Structural Elements During the 2016 Central Italy Earthquake." *Bulletin of Earthquake Engineering* 17 (10): 5655–5677. <https://doi.org/10.1007/s10518-018-0361-5>.
- Retamales, R., R. Davies, G. Mosqueda and A. Filiatrault. 2011. *Experimental Seismic Evaluation, Model Parametrization and Effects of Cold-Formed Steel-Framed Gypsum Partition Walls on the Seismic Performance of an Essential Facility*. Technical Report MCEER-11-0005. Buffalo, New York.
- Retamales, R., R. Davies, G. Mosqueda, and A. Filiatrault. 2013. "Experimental Seismic Fragility of Cold-Formed Steel Framed Gypsum Partition Walls." *Journal of Structural Engineering* 139 (8): 1285–1293. [https://doi.org/10.1061/\(asce\)st.1943-541x.0000657](https://doi.org/10.1061/(asce)st.1943-541x.0000657).
- Ricci, P., F. de Luca, and G. M. Verderame. 2011. "6th April 2009 L'Aquila Earthquake, Italy: Reinforced Concrete Building Performance." *Bulletin of Earthquake Engineering* 9 (1): 285–305. <https://doi.org/10.1007/s10518-010-9204-8>.
- Shahnazaryan, D., and G. O'Reilly. 2022. *XGBoost-Models-for-Demand-Intensity-Models*. <https://doi.org/10.5281/zenodo.6844842>.
- Shahnazaryan, D., G. J. O'Reilly, and R. Monteiro. 2022. "On the Seismic Loss Estimation of Integrated Performance-Based Designed Buildings." *Earthquake Engineering and Structural Dynamics*, (January): 1–25. <https://doi.org/10.1002/eqe.3638>.
- Stewart, W. G. 1987. *The Seismic Design of Plywood Sheathed Shearwalls*. Christchurch: Department of Civil Engineering, University of Canterbury.

- Taghavi, S., E. Miranda. 2004. "Estimation of Seismic Acceleration Demands in Building Components." 13th World Conference on Earthquake Engineering Vancouver, BC, Canada.
- Vamvatsikos, D. 2013. "Derivation of New SAC/FEMA Performance Evaluation Solutions with Second-Order Hazard Approximation." *Earthquake Engineering & Structural Dynamics* 42 (8): 1171–1188. <https://doi.org/10.1002/eqe.2265>.
- Veletsos, A. S., N. M. Newmark. 1960. "Effects of Inelastic Behavior on the Response of Simple System to Earthquake Motions." In *Proceedings of the 2nd World Conference on Earthquake Engineering*. Japan.
- Wanitkorkul, A., and A. Filiatroult. 2008. "Influence of Passive Supplemental Damping Systems on Structural and Nonstructural Seismic Fragilities of a Steel Building." *Engineering Structures* 30 (3): 675–682. <https://doi.org/10.1016/j.engstruct.2007.05.013>.
- Woessner, J., and S. Wiemer. 2005. "Assessing the Quality of Earthquake Catalogues: Estimating the Magnitude of Completeness and Its Uncertainty." *Bulletin of the Seismological Society of America* 95 (2): 684–698. <https://doi.org/10.1785/0120040007>.
- Wolpert, D. 1992. "Stacked Generalization (Stacking)." *Neural Networks* 5 (2): 241–259. [https://doi.org/10.1016/S0893-6080\(05\)80023-1](https://doi.org/10.1016/S0893-6080(05)80023-1).
- Zhang, Y., H. V. Burton, H. Sun, and M. Shokrabadi. 2018. "A Machine Learning Framework for Assessing Post-Earthquake Structural Safety." *Structural Safety* 72:1–16. <https://doi.org/10.1016/j.strusafe.2017.12.001>.
- Zhang, R., Z. Chen, S. Chen, J. Zheng, O. Büyüköztürk, and H. Sun. 2019. "Deep Long Short-Term Memory Networks for Nonlinear Structural Seismic Response Prediction." *Computers and Structures* 220:55–68. <https://doi.org/10.1016/j.compstruc.2019.05.006>.
- Žižmond, J., and M. Dolšek. 2019. "Formulation of Risk-Targeted Seismic Action for the Force-Based Seismic Design of Structures." *Earthquake Engineering & Structural Dynamics* 48 (12): 1406–1428. <https://doi.org/10.1002/eqe.3206>.